

1 Stabilized Supralinear Network: Model of Layer 2/3 of 2 the Primary Visual Cortex

3 Dina Obeid^{*1,2} and Kenneth D. Miller^{†1,3}

⁸ ²Harvard John A. Paulson School Of Engineering And Applied Sciences,
⁹ Harvard University, Cambridge, MA 02138, USA

10 ³Department of Neuroscience and Kavli Institute for Brain Science, College
11 of Physicians and Surgeons and Mortimer B. Zuckerman Mind Brain
12 Behavior Institute, Columbia University, New York City, NY, USA

13 December 30, 2020

14 **Abstract**

15 Electrophysiological recording in the primary visual cortex (V1) of mammals have
16 revealed a number of complex interactions between the center and surround. Under-
17 standing the underlying circuit mechanisms is crucial to understanding fundamental

*dinaobeid@seas.harvard.edu

[†]ken@neurotheory.columbia.edu

18 brain computations. In this paper we address the following phenomena that have been
19 observed in V1 of animals with orientation maps: 1) surround suppression that is ac-
20 companied by a decrease in the excitatory and inhibitory currents that the cell receives
21 as the stimulus size increases beyond the cell's summation field; 2) surround tuning
22 to the center orientation, in which the strongest suppression arises when the surround
23 orientation matches that of the center stimulus; and 3) feature-specific suppression, in
24 which a surround stimulus of a given orientation specifically suppresses that orienta-
25 tion's component of the response to a center plaid stimulus. We show that a stabilized
26 supralinear network that has biologically plausible connectivity and synaptic efficacies
27 that depend on cortical distance and orientation difference between neurons can con-
28 sistently reproduce all the above phenomena. We explain the mechanism behind each
29 result, and argue that feature-specific suppression and surround tuning to the center
30 orientation are independent phenomena. Specifically, if we remove some aspects of
31 the connectivity from the model it will still produce feature-specific suppression but
32 not surround tuning to the center orientation. We also show that in the model the
33 activity decay time constant is similar to the cortical activity decay time constant re-
34 ported in mouse V1. Our model indicates that if the surround activates neurons that
35 fall within the reach of the horizontal projections in V1, the above mentioned phe-
36 nomena can be generated by V1 alone without the need of cortico-cortical feedback.
37 Finally, we show that these results hold both in networks with rate-based units and
38 with conductance-based spiking units. This demonstrates that the stabilized supra-
39 linear network mechanism can be achieved in the more biological context of spiking
40 networks.

41 **Introduction**

42 Electrophysiological recording from cells in the primary visual cortex (V1) reveal that visual
43 stimuli presented outside the classical receptive field (CRF) of a neuron (the surround) can
44 modulate the neuron's response to a stimulus present in its CRF (the center) in complex

45 ways. The degree and direction of modulation depends on the distance between the center
46 and surround, the contrasts of the stimuli, their relative orientations, etc. (Akasaki et al.,
47 2002; Bair et al., 2003; Cavanaugh et al., 2002; Sceniak et al., 1999; Shen et al., 2007; Sillito
48 et al., 1995; Wang et al., 2009). Which of these modulations are carried by V1 lateral
49 connections, and which require top-down signals from higher visual areas is still largely
50 unknown. Understanding the underlying circuit mechanisms is crucial to understanding
51 fundamental brain computations.

52 To address these mechanisms, we build a spatially-extended, biologically-constrained
53 model of layer 2/3 of V1 of animals with orientation maps. We investigate whether a set
54 of key phenomena that have been reported in V1 can be consistently generated by lat-
55 eral connections alone, without the need of cortico-cortical feedback. We find that lateral
56 connections are sufficient provided that specific conditions for connectivity and synaptic ef-
57 ficacies are met. Therefore, our model makes testable predictions about the structure of the
58 underlying circuit.

59 We first address surround suppression. We show that our model can successfully repro-
60 duce surround suppression in similar strength and with similar contrast dependence to that
61 observed in layer 2/3 of V1 of animals with orientation maps. Furthermore, this suppression
62 is accompanied by a decrease in both excitatory and inhibitory conductances that the cell
63 receives, as reported in Ozeki et al. (2009). In order to achieve this, in addition to structured
64 connectivity, the network must locally have strong connections. Although many studies have
65 shown that surround suppression in V1 can be mediated through lateral connections (Ru-
66 bin et al., 2015), this is the first demonstration of the accompanying decrease in received
67 inhibition as well as excitation in a spatially extended (spatially two-dimensional) model.

68 We then investigate two new phenomena: (1) The strongest suppression arises when the
69 surround orientation matches that of the center stimulus, even when the center orientation
70 is not optimal for the cell (Shushruth et al., 2012; Trott and Born, 2015) and (2) A surround
71 with orientation matching the orientation of one component of a plaid center stimulus more

72 strongly suppresses the response of the matching component (Trott and Born, 2015). We
73 show that phenomena (1) and (2) can be generated within V1 if the surround falls with the
74 reach of V1 lateral connections. We find that to match (1), local connectivity, in addition to
75 being strong, must be broadly tuned for orientation; however to match (2) this additional
76 requirement is not needed. This leads us to conclude that effects (1) and (2) are independent.

77 We further show that in the model the activity decay time constant is fast, similar to
78 the cortical activity decay time constant reported by Reinhold et al. (2015). Finally, we
79 show that our results hold in networks with conductance-based spiking units as well as rate
80 units. This demonstrates that the Stabilized-Supralinear Network mechanism described in
81 Ahmadian et al. (2013) and Rubin et al. (2015) can arise in the more biological context of a
82 spiking neural network (see also Sanzeni et al. (2020a,b)).

83 Model

84 Model Overview

85 To investigate the computational role of V1 lateral connections, we build a 2-dimensional
86 spatially extended model of layer 2/3 of the primary visual cortex of animals with orientation
87 maps. Retinotopic position changes smoothly across both spatial dimensions, while preferred
88 orientation of neurons is determined by their position in the orientation map. The Cortical
89 Magnification Factor (CMF), which expresses how many mm of cortex represents one degree
90 in visual angle, constrains the size of a neuron's receptive field (RF), as we describe below.

91 The connectivity in the model is broadly constrained by biological data. Neurons in V1
92 layer 2/3 are found to form dense axonal projections at distances of a few hundred μm , and
93 sparse long range horizontal projections that target cells of similar orientation preferences.
94 These long range connections, which can reach up to 3 mm in cat and 10 mm in monkey, arise
95 from excitatory cells, and give rise to the patchy connectivity observed in V1 (Amir et al.,
96 1993; Bosking et al., 1997; Stettler et al., 2002). In comparison, inhibitory cells primarily

97 form short range connections.

98 We first present results from a rate-based model. The units in the rate-based model
99 are taken to have an expansive or supralinear, power-law transfer function (Albrecht and
100 Hamilton, 1982; Albrecht, 1991; Carandini et al., 1997, 1999; Finn et al., 2007; Hansel
101 and Van Vreeswijk, 2002; Heeger, 1992; Miller and Troyer, 2002), as expected for neurons
102 whose spiking is driven by input fluctuations rather than by the mean input (Hansel and
103 Van Vreeswijk, 2002; Miller and Troyer, 2002). Rubin et al. (2015) and Ahmadian et al.
104 (2013) showed that when neural-like units have such a power-law transfer function, responses
105 with nonlinear behaviors observed in visual cortex emerge due to network dynamics. The
106 authors called this mechanism the Stabilized Supralinear Network (SSN). They showed that
107 the SSN mechanism can explain normalization and surround suppression and their nonlin-
108 ear dependencies on stimulus contrast, which are observed across multiple sensory cortical
109 areas.

110 To verify that our results are robust and independent of the neuron model, we also build
111 a conductance-based spiking neural network model, and show that all our key results still
112 hold. This shows as well that the SSN mechanism can be realized with spiking neurons.

113 Model Details

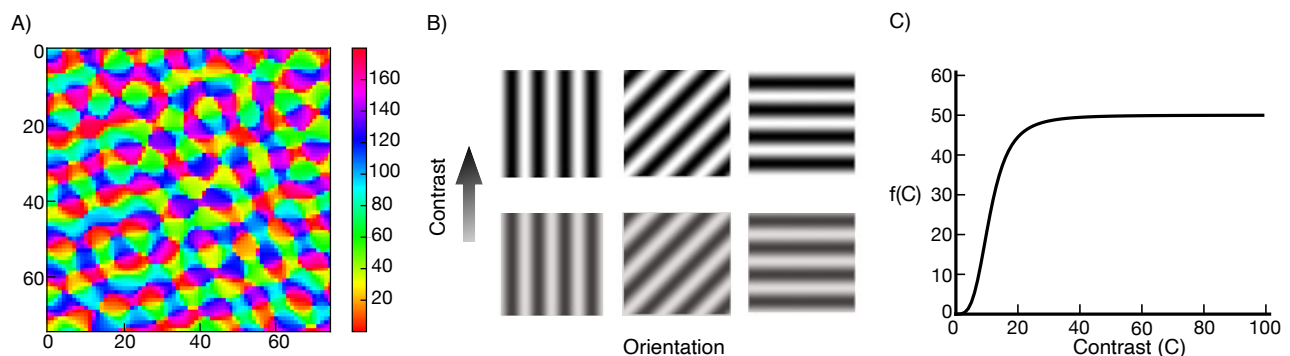


Figure 1: (A) Orientation map, the color corresponds to the cells preferred orientation. (B) Gratings with different orientations and contrasts. (C) External input as a function of the stimulus contrast (Eq. 3).

114 We use a grid of 75 x 75 grid points. We place one excitatory cell (E), and one inhibitory
115 cell (I) at each location on the lattice, and thus have 5625 E cells and 5625 I cells in the
116 network. Even though we use a 50/50 E/I ratio, we believe that our main results will
117 not change if we take the E/I ratio to be 80/20. In unpublished work we studied SSN
118 behavior in spiking networks consisting of 1152 E cells and 288 I cells (E/I ratio of 80/20),
119 and found that the network behavior was consistent with SSN predictions in the parameter
120 regime we studied (strongly suppressive regime, *i.e.* with $\Omega_E < \Omega_I < 0$, using parameters
121 defined in Ahmadian et al. (2013)). We take the map to represent 16x16 degrees of visual
122 space, with position in visual space varying linearly across the map, and assume a Cortical
123 Magnification Factor (CMF) of 0.5 mm/deg. Thus the grid represents 8.0 x 8.0 mm of
124 cortex, with each grid interval representing 0.213 degrees and 107 μm of cortical distance.
125 We use periodic boundary conditions; our results are independent of that condition. This is
126 verified by removing periodic boundary conditions, and adjusting the weight efficacy matrix
127 to compensate for the lost connections.

128 We superpose on the grid an orientation map, specifying the preferred orientations of cells
129 at the corresponding grid points (Fig. 1A). The orientation map is generated randomly using
130 the method described in Kaschube et al. (2010) (their supplementary materials, Eq. 20). To
131 summarize, we superpose n complex plane waves to form a function $z(\mathbf{x})$ of two-dimensional
132 spatial position \mathbf{x} :

$$133 \quad z(\mathbf{x}) = \sum_{j=1}^n e^{i(l_j \mathbf{k}_j \cdot \mathbf{x} + \phi_j)}. \quad (1)$$

134 Here, $\mathbf{k}_j = k(\cos(j\pi/n), \sin(j\pi/n))$, with signs $l_j \in \{+1, -1\}$ and phases $\phi_j \in [0, 2\pi)$
135 randomly chosen. Writing $z(\mathbf{x}) = r(\mathbf{x})e^{i\Phi(\mathbf{x})}$ for real amplitude $r(\mathbf{x})$ and phase $\Phi(\mathbf{x})$, we take
136 the preferred orientation at each grid point \mathbf{x} to be $\Phi(\mathbf{x})/2$. We use a map spatial frequency
137 of $k = \frac{8 \text{ cycles}}{75 \text{ grid points}}$, *i.e.* a map with on average 8 full periods of the orientation map across
138 the length or width of the grid, and $n = 30$. The orientation map is not periodic, so there is
139 a discontinuity in orientation at the grid borders, although the retinotopy and intracortical

140 connections wrap around. In our results, we report on cells sampled away from the boundary
141 ($20 < x < 60, 20 < y < 60$, in terms of the grid coordinates that go from 1 to 75 in each
142 dimension) to avoid boundary effects.

143 The excitatory cells form long range connections, while the inhibitory cells form short
144 range connections. The connection strength from a unit of type Y and grid position b
145 to a unit of type X at position a , $X, Y \in \{E, I\}$, is written W_{XY}^{ab} . Let the units at a
146 and b have positions \mathbf{x}_a and \mathbf{x}_b , respectively, and preferred orientations θ_a and θ_b . The
147 connection strength is given by $W_{XY}^{ab} = J_{XY} p_{XY}(|\mathbf{x}_a - \mathbf{x}_b|) q_{XY}(d(\theta_a, \theta_b))$, where $d(\theta_a, \theta_b)$ is
148 the shortest angular distance around a 180° circle between the two orientations. Here, $p_{XY}(x)$
149 describes the dependence of strength on the spatial distance between the units (measured
150 as the shortest distance across the grid with periodic boundary conditions), while $q_{XY}(\theta)$
151 describes the dependence on the difference between their preferred orientations measured
152 as shortest distance around the circle of orientations . The function $p_{XY}(x)$ is specified
153 as follows: for projections of excitatory cells, $p_{XE}(x)$ is 1 for distances $x \leq L_o$, and then
154 decays as a Gaussian with standard deviation σ_{XE} . $L_o = 324 \mu\text{m}$, $\sigma_{EE} = 324 \mu\text{m}$ and
155 $\sigma_{IE} = 642 \mu\text{m}$. For projections of inhibitory cells, $p_{XI}(x)$ is Gaussian with standard deviation
156 $\sigma_{EI} = \sigma_{II} = 216 \mu\text{m}$. For all cells regardless of pre- or postsynaptic type, the function
157 $q_{XY}(\theta)$ has the form of a Gaussian with a non-zero baseline: $q_{XY}(\theta) = A_{XY} + B_{XY} e^{\frac{-\theta^2}{2 * (\sigma_{XY}^{ori})^2}}$.
158 For projections of I cells and of E cells at distances less than L_o , $A_{XI} = A_{XE} = 0.2$,
159 $B_{XI} = B_{XE} = 0.8$ and $\sigma_{XI}^{ori} = \sigma_{XE}^{ori} = 55^\circ$. For projections of excitatory cells at distances
160 greater than L_o , $A_{XE} = 0.14$, $B_{XE} = 0.86$ and $\sigma_{XE}^{ori} = 25^\circ$. The constants J_{XY} are, for I
161 projections, $J_{EI} = 0.0528$ and $J_{II} = 0.0288$; for E projections, at distances less than L_o ,
162 $J_{EE} = 0.072$ and $J_{IE} = 0.06$, while at distances greater than L_o , $J_{EE} = J_{IE} = 0.036$. We
163 point out that the heterogeneity in the network comes from the underlying orientation map.

164 We choose the connectivity parameters so that the connectivity profile agrees with exper-
165 imental findings. We choose the J_{XY} such that 1) the network is in a strong sublinear regime
166 (see Result 1 for more details) and 2) with increasing stimulus size, the loss of excitatory

167 input to inhibitory cells from nearby surround-suppressed excitatory cells is greater than
168 their gain in excitatory input from far away excitatory cells, which is necessary for the net
169 inhibition received by excitatory cells to decrease with surround suppression. We constrain
170 the rest of the model parameters by experimental data to make the model more biologically
171 plausible.

172 We ignore stimulus features like spatial frequency and phase, and consider only three
173 features: contrast, orientation and size (Fig. 1B). The cells in the model behave like ideal
174 complex cells, in that their response to a drifting grating is static in time. Spatially, each
175 cell has a circularly symmetric Gaussian receptive field with standard deviation $\sigma_{rf} = 0.09^\circ$.
176 The external input to a neuron located at position (x_o, y_o) with preferred orientation θ_o ,
177 from a stimulus of contrast C and orientation θ_s that is centered at (x_s, y_s) and is uniform
178 for a diameter of ℓ degrees about the center (and zero contrast outside), is given by

179
$$f(C) h_\ell(\mathbf{x}_s - \mathbf{x}_o) g(\theta_s - \theta_o). \quad (2)$$

180 Here $f(C)$ is a Naka-Rushton function given by

181
$$f(C) = \frac{f_{max} * C^{3.5}}{C_{50}^{3.5} + C^{3.5}} \quad (3)$$

182 with $f_{max} = 50$ and $C_{50} = 11$ (Fig. 1C). $h_\ell(\mathbf{x})$ is the integral of the product of the Gaussian
183 classical receptive field with a sharp edge stimulus. It is given by:

184
$$h_\ell(\mathbf{x}_s - \mathbf{x}_o) = \frac{1}{4} \left(\operatorname{erf} \left(\frac{\ell/2 + (x_s - x_o)}{\sigma_{rf} \sqrt{2}} \right) + \operatorname{erf} \left(\frac{\ell/2 - (x_s - x_o)}{\sigma_{rf} \sqrt{2}} \right) \right) * \left(\operatorname{erf} \left(\frac{\ell/2 + (y_s - y_o)}{\sigma_{rf} \sqrt{2}} \right) + \operatorname{erf} \left(\frac{\ell/2 - (y_s - y_o)}{\sigma_{rf} \sqrt{2}} \right) \right) \quad (4)$$

185 where $\operatorname{erf}(x)$ is the error function defined as $\operatorname{erf}(x) = \frac{1}{\sqrt{\pi}} \int_{-x}^x e^{-t^2} dt$. The function g is defined

186 by

187

$$g(\theta_s - \theta_o) = e^{\frac{-d(\theta_s, \theta_o)^2}{2 * \sigma_{fori}^2}} \quad (5)$$

188 with $\sigma_{fori} = 20^\circ$. To define the equations for the rate model, we let r_E^a be the rate of the
 189 excitatory neuron at position a , and r_I^a similarly. Both receive the same external input I_{Ext}^a .
 190 The rate equations are:

191

$$\begin{aligned} \tau_E \frac{dr_E^a}{dt} &= -r_E^a + K[I_{Ext}^a + \sum_b W_{EE}^{ab} r_E^b - \sum_b W_{EI}^{ab} r_I^b]_+^{n_E} \\ \tau_I \frac{dr_I^a}{dt} &= -r_I^a + K[I_{Ext}^a + \sum_b W_{IE}^{ab} r_E^b - \sum_b W_{II}^{ab} r_I^b]_+^{n_I} \end{aligned} \quad (6)$$

192 where $[x]_+ = \max(0, x)$. The excitatory cells' time constant $\tau_E = 10\text{ ms}$, and the inhibitory
 193 cells' time constant $\tau_I = 6.67\text{ ms}$. We use, $K = 0.01$, $n_E = n_I = 2.2$. $\sum_b W_{XE}^{ab} r_E^b$ is the
 194 recurrent excitatory input to neuron X^a where $X = \{E, I\}$. Similarly, $\sum_b W_{XI}^{ab} r_I^b$ is the
 195 recurrent inhibitory input.

196 For the conductance-based model, the equations of motion of the membrane potential
 197 and the conductances for each cell are identical for E and I cells. For a cell at a of type X ,
 198 the equations are (we omit specifying the type X for the dynamical variables and parameters
 199 that don't differ between the two types):

200

$$\begin{aligned} \tau_m \frac{dV^a}{dt} &= -(V^a - R_L) + \frac{g_E^a}{g_L} (R_E - V^a) + \frac{g_I^a}{g_L} (R_I - V^a) + \frac{g_{in}^a}{g_L} (R_E - V^a) + \sigma_V \sqrt{2\tau_m} \eta^a(t) \\ \tau_E \frac{dg_E^a}{dt} &= -g_E^a + \tau_E \sum_{b=1}^{N_E} \sum_j g_{XE}^{ab} \delta(t - t_{Ej}^b) \\ \tau_I \frac{dg_I^a}{dt} &= -g_I^a + \tau_I \sum_{b=1}^{N_I} \sum_j g_{XI}^{ab} \delta(t - t_{Ij}^b) \\ \tau_E \frac{dg_{in}^a}{dt} &= -g_{in}^a + \bar{g}_{in}^a + \sqrt{\tau_E} \sigma_{g_{in}}^a \zeta^a(t). \end{aligned} \quad (7)$$

201 Here V^a is the membrane potential of the given cell at a . τ_m is the membrane potential
 202 time constant. g_E^a is the excitatory AMPA-like conductance, g_I^a is the inhibitory GABA-like

203 conductance and g_{in}^a is the excitatory input conductance from outside the network. R_E ,
 204 R_I , and R_L are reversal potentials of the excitatory, inhibitory, and leak conductances. τ_E
 205 and τ_I are the time constants of the excitatory and inhibitory conductances. g_{XE}^{ab} is the
 206 conductance of the synapse of the excitatory cell at b to the given cell at a , similarly g_{XI}^{ab}
 207 is the conductance from the inhibitory cell at b , and t_{Xj}^b is the time of the j^{th} spike of the
 208 cell of type X at b . $\delta(x)$ is the Dirac delta function. Each cell in the network receives input
 209 from N_{input} external spiking cells, where N_{input} is a large number. We assume the spike
 210 trains are Poisson and invoke the Central Limit Theorem to approximate the input to the
 211 cell $\tau_E g_{ext} \sum_{i=1}^{N_{input}} \sum_k \delta(t - t_i^k)$ by a stochastic process with mean \bar{g}_{in}^a and variance $\tau_E \sigma_{g_{in}}^{a^2}$,
 212 where ζ^a is white Gaussian noise with $\langle \zeta^a(t) \zeta^a(t') \rangle = \delta(t - t')$. The stochastic dynamics
 213 will lead g_{in}^a to have a mean \bar{g}_{in}^a and a variance $\sigma_{g_{in}}^{a^2}/2$ (Tuckwell, 1988), where

$$214 \quad \begin{aligned} \bar{g}_{in}^a &= N_{input} r_{ext} \tau_E g_{ext} \\ \sigma_{g_{in}}^{a^2} &= N_{input} r_{ext} \tau_E g_{ext}^2 \end{aligned} \quad (8)$$

215 where g_{ext} is the amplitude of the conductance evoked when a single external cell spikes,
 216 and r_{ext} is the firing rate of the external cells given by Eq. 2. We assume the membrane
 217 potential is noisy, and model the noise as white Gaussian noise. $\eta^a(t)$ is a Gaussian random
 218 variable with mean 0 and variance 1, and σ_V is the standard deviation of the membrane
 219 potential fluctuations. In the simulations we set $\sigma_V = 6.85 \text{ mV}$ to get spontaneous activity
 220 similar to what has been reported in (Chen et al., 2009; Gur and Snodderly, 2008; Ringach
 221 et al., 2002). In the model the mean spontaneous activity of the excitatory cells is about
 222 1.5 Hz, and of the inhibitory cells is about 3 Hz. The parameters for both E and I cells are
 223 as follows: $\tau_m = 15 \text{ ms}$; $\tau_E = \tau_I = 3 \text{ ms}$; $R_L = -70 \text{ mV}$; $R_E = 0 \text{ mV}$; $R_I = -80 \text{ mV}$;
 224 $g_L = 10 \text{ nS}$; $N_{input} = 200$ and $g_{ext} = 0.1 \text{ nS}$. We take threshold voltage $V_{th} = -50 \text{ mV}$ and
 225 after-spike rest voltage to be 6 mV below threshold, $V_r = -56 \text{ mV}$, as in Troyer and Miller
 226 (1997). After the cell spikes, it goes into a refractory period with $\tau_{ref} = 3 \text{ ms}$.

227 Similar to the rate model, the conductance values are given by $g_{XY}^{ab} = g_{XY} p_{XY} (|\mathbf{x}_a -$

228 $\mathbf{x}_b|)q_{XY}(d(\theta_a, \theta_b))$. The parameters g_{XY} are: $g_{EI} = 3.3 \text{ } nS$ and $g_{II} = 2 \text{ } nS$; at distances less
229 than L_o , $g_{EE} = 1.8 \text{ } nS$ and $g_{IE} = 1.76 \text{ } nS$; and at distances greater than L_o , $g_{EE} = 0.7 \text{ } nS$
230 and $g_{IE} = 0.65 \text{ } nS$. Again $L_o = 324 \mu\text{m}$ as in the rate model.

231 To measure the strength of the surround suppression in the network, we compute the
232 suppression index (SI) defined as:

233
$$SI = \frac{r_{max} - r_{inf}}{r_{max}} \quad (9)$$

234 where r_{max} is the response to a stimulus size that elicits maximum response, and r_{inf} is the
235 response for a very large stimulus. To measure whether the presence of a surround stimulus
236 facilitates or suppresses the response of a cell compared to its response to a center-only
237 stimulus, we define a modified suppression index:

238
$$SI_m = \frac{r_{(center-only)} - r_{(center+surround)}}{r_{(center-only)}} \quad (10)$$

239 SI_m negative means facilitation, while SI_m positive means suppression.

240 In experiments on the surround tuning to the center orientation, we fix the center stimulus
241 diameter, and the inner and outer annulus diameters to $(1.3^\circ, 4.3^\circ, 21.6^\circ)$ and set both stimuli
242 contrasts to 100. In these experiments we record the activity of a single neuron as we vary
243 the stimulus orientations, and we roughly pick the largest annulus inner diameter at which
244 the phenomena is still observed. This corresponds to an annulus inner radius of 2.15° or
245 1.1 mm which is roughly the span of E-to-I monosynaptic connections. In feature-specific
246 suppression experiments we fix the center stimulus diameter, and the inner and outer annulus
247 diameters to $(1.7^\circ, 3.9^\circ, 21.6^\circ)$. In these experiments we follow the procedure in Trott and
248 Born (2015) to make our results directly comparable with experimental data. Thus, we use
249 a slightly bigger center stimulus to obtain a better fit of the population rates (see Result
250 3 for more details). The contrast is set to 16.4 (representing 80% of the maximal input
251 strength), for each component of the plaid as well as the surround in the rate model, and to

252 50 (representing 99.5% of the maximal input) in the conductance-based model.

253 In all experiments, cells are sampled randomly from locations away from the boundary.

254 We first randomly pick 100 locations within the region we define as away from the boundary

255 ($20 < x < 60, 20 < y < 60$). Cells in all experiments are randomly picked from those 100

256 locations.

257 Results

258 We first check that our network is functioning as an SSN, by checking for several salient

259 SSN behaviors. The SSN shows a transition, with increasing input strength, from a weakly

260 coupled, largely feedforward driven regime for weak external input, to a strongly coupled,

261 recurrently-dominated regime for stronger external input (Ahmadian et al., 2013). This

262 transition can account for many aspects of summation of responses to two stimuli and of

263 center-surround interactions and their dependencies on stimulus contrast (Rubin et al., 2015).

264 Our network shows the characteristic signs of this transition (Rubin et al., 2015): the net

265 input a neuron receives grows linearly or supralinearly as a function of external input for

266 weak external input, but sublinearly for stronger external input (Fig. 2A); this net input is

267 dominantly external input for weak external input, but network-driven input for stronger

268 external input (Fig. 2B); the network input becomes increasingly inhibitory with increasing

269 external drive (Fig. 2C); and a surround stimulus of a fixed contrast can be facilitating for

270 a weak center stimulus, but becomes suppressive for stronger external drive to the center

271 (Fig. 2D).

272 We then explore whether lateral connections in V1 are capable of generating several

273 phenomena that emerge due to center-surround interaction.

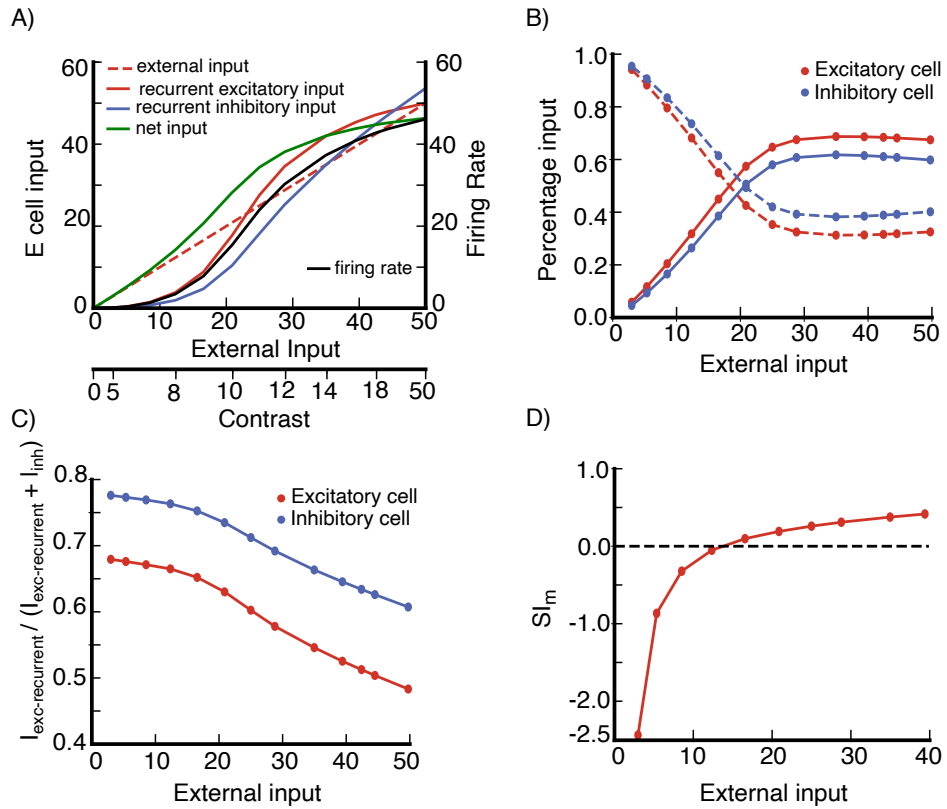


Figure 2: Stabilized Supralinear Network (SSN) behavior of the model network (A)
 Inputs to an excitatory (E) cell and its firing rate vs external input, the cell is at a randomly selected grid location (see section Model Details). Stimulus contrast level corresponding to external input is shown on the bottom axis. The net input is defined as $(I_{ext} + I_{exc\text{-recurrent}} - I_{inh})$, where I_{ext} is the external input to the cell, $I_{exc\text{-recurrent}}$ is the cell's recurrent excitatory input from the network, and I_{inh} its recurrent inhibitory input from the network, I_{inh} is defined to be positive, see section Model Details for the expressions of $I_{exc\text{-recurrent}}$ and I_{inh} . (B) Percentage of external and network inputs as a function of external input for the excitatory cell in (A) and an inhibitory cell at the same grid location (dashed line is external input, solid line is network input). Here, the total input is defined as $(I_{ext} + I_{exc\text{-recurrent}} + I_{inh})$, and the network input is $(I_{exc\text{-recurrent}} + I_{inh})$. (C) $I_{exc\text{-recurrent}} / (I_{exc\text{-recurrent}} + I_{inh})$ as a function of external input for the excitatory and inhibitory cells in (A,B). In panels (A-C) we use a stimulus of diameter 2.16° centered on the cell's retinotopic position and with the cell's preferred orientation. (D) Surround Facilitation to Suppression transition: a near surround can be facilitating or suppressing depending on the center stimulus contrast. SI_m negative means facilitation, while SI_m positive means suppression (see section Model Details, Eq. 10 for the definition of SI_m). In panel (D) the data is from an excitatory cell at a randomly selected grid location (see section Model Details); surround stimulus has contrast $C = 12$, and inner and outer diameters 0.865° and 4.32° respectively; the center stimulus diameter is 0.65° ; both center and surround stimuli are centered on the cell's retinotopic position, with the cell's preferred orientation.

274 Result 1: Surround Suppression

275 We first investigate surround suppression, a widely studied phenomena in V1 and other
276 sensory areas in multiple species (Angelucci et al., 2017). Ozeki et al. (2009) showed in
277 anesthetized cat V1 that, after presenting an optimal center-only stimulus, presentation of
278 an iso-oriented surround stimulus decreased firing rates, and decreased both the inhibition
279 and excitation neurons receive. Adesnik (2017) similarly showed that inhibition as well as
280 excitation were decreased by surround suppression in awake mice. Ozeki et al. (2009)
281 showed that suppression of inhibition as well as excitation required that the network be
282 an *inhibition stabilized network*, or ISN, meaning that, if inhibition were frozen and could
283 not respond dynamically, the excitatory subnetwork would be unstable. Rubin et al. (2015)
284 demonstrated a circuit model with one spatial dimension in which surround suppression
285 was accompanied by a decrease of inhibition as well as excitation, and showed contrast
286 dependence like that seen in visual cortex. They also studied a model with two spatial
287 dimensions that was in a different parameter regime but that showed similar behaviors.
288 However, since Rubin et al. (2015) was published, we discovered that the 2-D spatial model
289 of V1 studied there did not show a decrease in inhibition received with surround suppression,
290 and to our knowledge no other 2-D spatial model of V1 has shown this. We investigate the
291 conditions under which surround suppression can emerge in a 2-d spatially extended model
292 of layer 2/3 of V1 with a decrease in inhibition received. More specifically, what structure of
293 connectivity and synaptic efficacies can achieve this? Before addressing this question, we first
294 show that our model replicates surround suppression behavior and its contrast dependence
295 observed in Rubin et al. (2015).

296 To study surround suppression, we record the firing rates of a cell in the network, as
297 we vary the diameter of a high contrast stimulus centered on the cell's retinotopic position
298 and with orientation identical to the recorded cell's preferred orientation. In the model both
299 excitatory (E) and inhibitory (I) cells are surround-suppressed. However, excitatory cells
300 are more strongly surround suppressed than inhibitory cells, as illustrated by an E and I

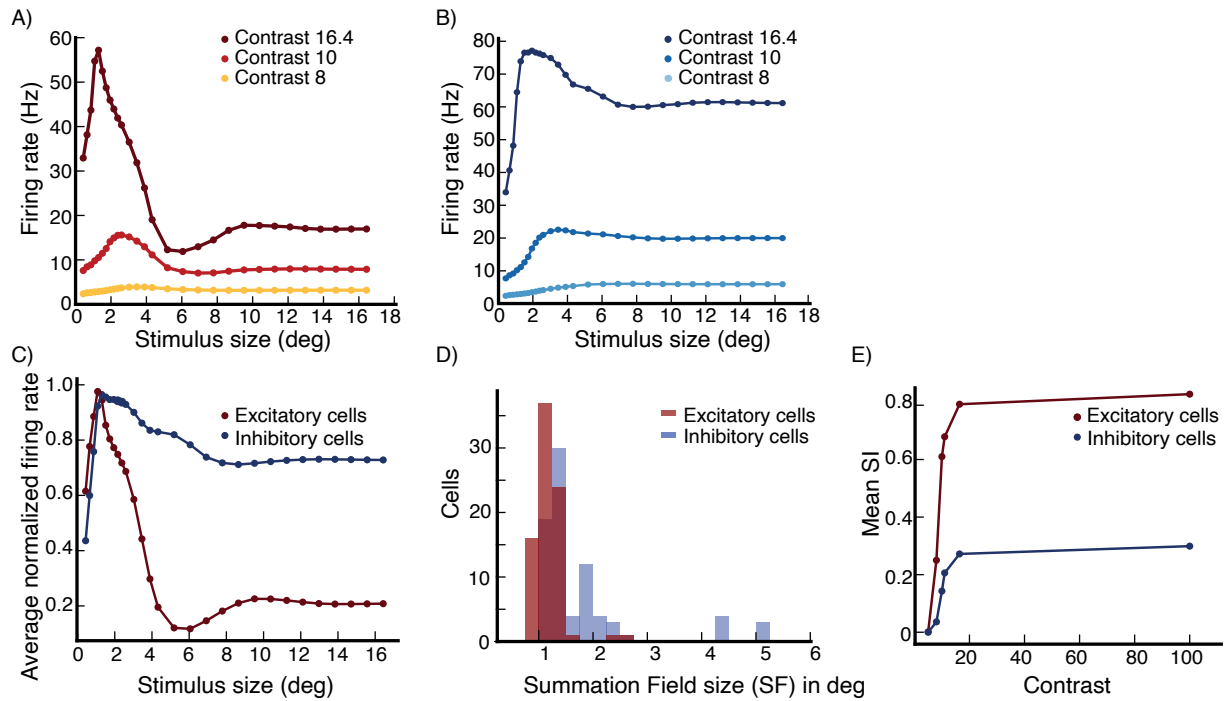


Figure 3: Surround suppression (A,B) The firing rates of an excitatory (E) cell (A) and an inhibitory (I) cell at the same grid location (B) vs. stimulus size. Different colors correspond to different stimulus contrast levels, high ($C=16.4$; external input 80% of maximal), medium ($C=10$; external input 42% of maximal) and low ($C=8$; external input 25% of maximal). The cells are at a randomly selected grid location (see section Model Details). (C) The average firing rate of 80 E cells at randomly selected grid locations (see section Model Details), and of 80 I cells at the same grid locations, after normalizing each cell's rates so that its peak rate is 1.0, vs. stimulus size for a high contrast stimulus ($C=16.4$). (D) The distribution of Summation Field sizes (SFS) of the E and I cells used to produce panel (C), the mean SFS for the E cells is 1.14 deg and for the I cells is 1.75 deg. (E) The mean suppression index of the E cells and I cells used to produce panel (C) versus stimulus contrast, the mean Suppression Index (SI) for E and I cells changes from little or no suppression (low SI's) for very weak stimuli, to stronger suppression (higher SI's) for stronger stimuli, with E cells showing much stronger suppression than I cells. The error bars are too small to show properly, they are of order 10^{-2} or smaller.

301 cell at a randomly selected grid location (see section Model Details) (Fig. 3A,B) and by the
302 average size tuning across 80 E and 80 I cells (Fig. 3C) for a high contrast stimulus, $C=16.4$.
303 Accordingly, the summation field sizes – the size of a stimulus driving optimal response,
304 before further increase in size causes response suppression – of E cells are smaller than those
305 for I cells (Fig. 3D).

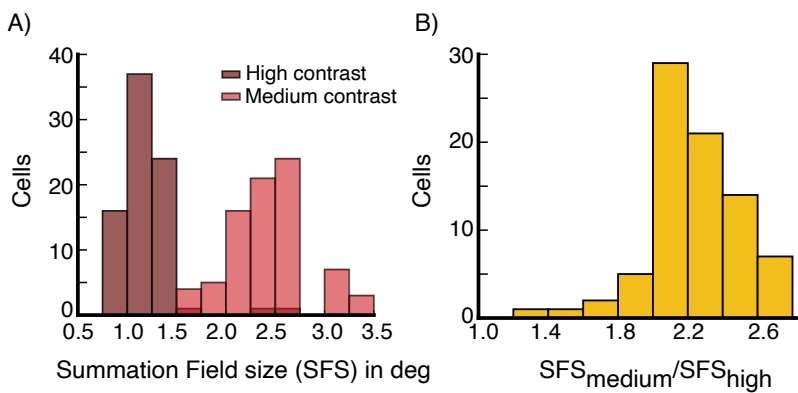


Figure 4: Surround suppression, summation field sizes (A) The distribution of summation field sizes for 80 excitatory (E) cells (same E cells used to produce panel Fig. 3C), at contrast $C=16.4$ (dark red color) and contrast $C=10$ (light red color). (B) The distribution of the ratio of the summation field sizes in (A). The summation field size of all cells is smaller for the higher contrast stimulus.

306 We repeat the above experiment with different contrast levels. The strength of surround
307 suppression increases with increasing stimulus contrast (Fig. 3A,B). The mean suppression
308 index (SI) increases from little or no suppression for weak contrasts to stronger suppression
309 for stronger contrasts (Fig. 3E). For a relatively high contrast stimulus ($C=16.4$, representing
310 80% of the maximal input strength), the mean suppression index (SI) is 0.79 for the E cells
311 and 0.27 for the I cells (where 0 is no suppression and 1 is complete suppression). Similarly,
312 the summation field size shrinks with increasing contrast, as we illustrate for E cells in
313 Fig. 4A,B, as in (Sceniak et al., 1999). The summation field sizes of I cells behave similarly.

314 We examine whether surround suppression in the network is accompanied by a decrease
315 in excitation and inhibition, as reported by Ozeki et al. (2009), rather than simply being
316 due to ramping up of inhibitory input. The size tuning of the excitatory and inhibitory
317 input currents to the E cell in Fig. 3A at high contrast ($C=16.4$) reveals that both currents

318 indeed show surround suppression (Fig. 5A). We then look at the average size tuning of
319 these currents across cells, after normalizing each cell's curve for each current to have a peak
320 of 1. Both E cells (Fig. 5B) and I cells (Fig. 5C) show surround suppression of both their
321 excitatory and their inhibitory currents.

322 We then wish to directly compare, across cells, the currents for a small, nearly-optimally-
323 sized stimulus to those for a large, suppressive stimulus. To compare to experiments, there
324 is now a problem to be solved: as modelers we know the exact stimulus size that gives peak
325 response, and can compare inhibition received for that size to inhibition received for a large
326 size. However experimenters do not know the optimal size, and must choose some size in that
327 vicinity, which may evoke less inhibition than the peak (see Fig. 3). Thus, if we choose the
328 optimal size for comparison, we may bias our results towards seeing a decrease in inhibition,
329 compared to experimental procedures. To avoid this, we follow a procedure similar to that
330 of Ozeki et al. (2009). We measure the excitatory and inhibitory inputs for a small stimulus
331 size with diameter d_s around which the cells respond close to maximally, and for a very large
332 stimulus at which all cells are surround suppressed. We take d_s to be equal to the median
333 of all stimulus diameters for which the sampled cells respond maximally. The results are
334 entirely similar if d_s is taken to be the mean rather than the median.

335 Using this procedure, for excitatory inputs and for inhibitory inputs to E and to I cells, we
336 plot the input current at small stimulus size vs. the current at large stimulus size (Fig. 5D,E).
337 In Fig. 5D we plot the excitatory inputs and inhibitory inputs respectively to 80 excitatory
338 cells, at small stimulus size against those at large stimulus size. Both excitatory and in-
339 hibitory inputs are smaller for the large suppressive stimulus. Fig. 5E shows the same data
340 for 80 inhibitory cells. Thus, for both excitatory and inhibitory cells in the model, surround
341 suppression is accompanied by a decrease in excitation and inhibition that the cell receives.

342 While we cannot exhaustively search all parameters, in our explorations of parameters,
343 we have found the surround suppression of inhibitory as well as excitatory input to depend
344 on two elements of the connectivity. First, locally, roughly over distances of about L_o (the

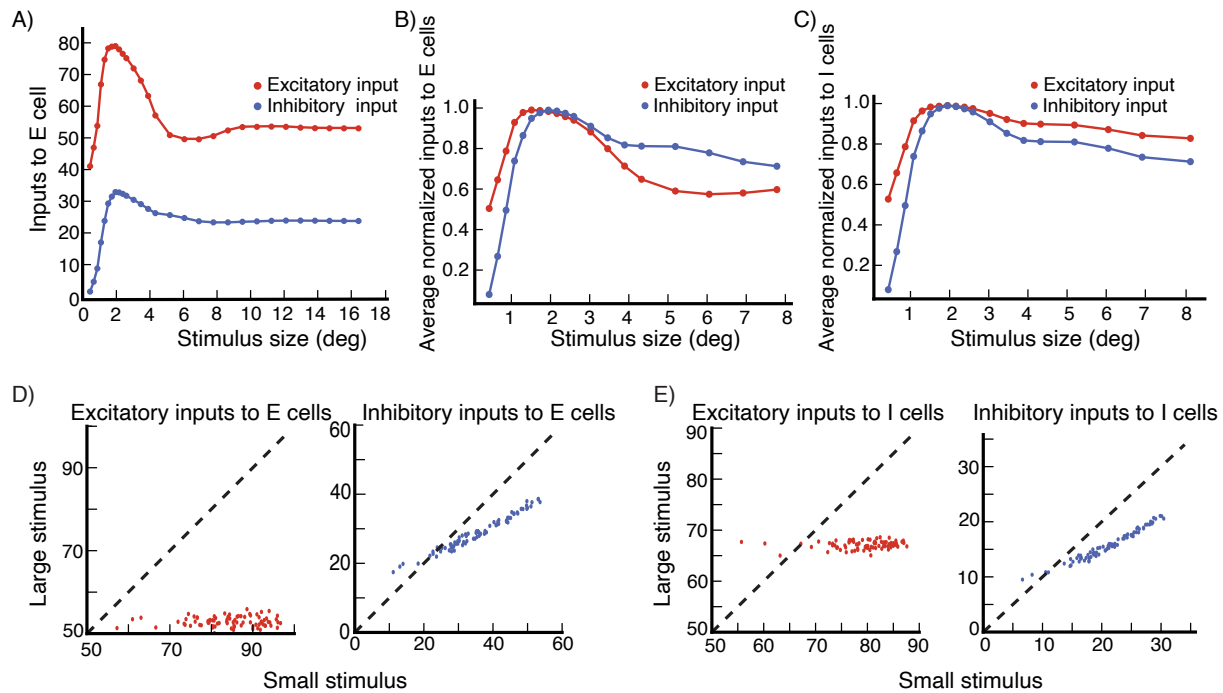


Figure 5: Surround suppression, inputs to cells (A) The excitatory (red) and inhibitory (blue) total input to the excitatory (E) cell in Fig. 3A, shown for the high contrast stimulus ($C=16.4$; external input 80% of maximal), both show surround suppression. (B,C) The size tuning of the averaged normalized excitatory and inhibitory inputs (each normalized to have peak value 1) to excitatory (E) cells (B) and inhibitory (I) cells (C) for contrast $C=16.4$ (same cells used to produce panel Fig. 3C). Note the change in horizontal axis between panels (A) and (B,C). (D) The excitatory and inhibitory inputs to E cells (same E cells used to produce panel Fig. 3C) for a large stimulus (for which all the cells are surround suppressed) are shown vs. their values for a small stimulus (with size given by the average size that yields maximal response across cells). Panel (E) is the same as (D) but for I cells (same I cells used to produce panel Fig. 3C). Stimulus contrast $C=16.4$.

345 distance over which lateral connections are most dense, see section Model Details), the
 346 cells must be strongly enough connected so that, as the stimulus size increases, the local
 347 circuit around the recorded cell goes through the SSN transition from being mainly driven
 348 by the feedforward input to being dominated by recurrent currents. This occurs through
 349 the increase in effective synaptic weights with increased external drive to the network due
 350 to the expansive, supralinear neuronal input/output function, which is the fundamental
 351 mechanism underlying the SSN (see (Ahmadian et al., 2013; Rubin et al., 2015) for a detailed
 352 description of the SSN mechanism). At the transition, the growth of effective excitatory
 353 synaptic strengths is sufficient that the excitatory subnetwork becomes unstable by itself

354 (Ahmadian et al., 2013), but the network is stabilized by feedback inhibition. This means
355 that the local circuit becomes an inhibition stabilized network (ISN), which was the condition
356 for surround suppression of inhibitory input identified in (Ozeki et al., 2009), based on the
357 ISN mechanism initially identified by (Tsodyks et al., 1997). We put the network into a
358 particular regime of the SSN that is thought to be most strongly non-linear, though we
359 don't know if this is necessary since we did not do an exhaustive parameter search. This
360 regime, using parameters defined in Ahmadian et al. (2013), is defined by $\Omega_E < 0$ (in
361 particular, we use $\Omega_E < 0 < \Omega_I$) where, for equal inputs to the excitatory and inhibitory
362 cells as we use here, $\Omega_E = W_{II} - W_{EI}$ and $\Omega_I = W_{IE} - W_{EE}$, with W_{XY} the total synaptic
363 weight from units of type Y to a unit of type X. This produces a regime in which responses
364 saturate with increasing external input (and ultimately would supersaturate for sufficiently
365 strong external input). In particular, for our connectivity parameters, $\Omega_E = -0.49 \pm 0.01$
366 and $\Omega_I = 3.59 \pm 0.03$.

367 The second element we have found critical is that the ratio of projection strength of long-
368 range horizontal connections to I cells vs. E cells must increase with increasing distance,
369 that is, the E-to-I connections must be effectively longer range than E-to-E connections.
370 Furthermore, the excitatory input received by I cells from far away E cells should not be
371 large compared to the excitatory input they receive from nearby excitatory cells. Then, with
372 increasing stimulus size, the loss of excitatory input to I cells from surround suppression of
373 nearby E cells can exceed the gain of excitatory input from far away E cells, causing the I
374 cells to be surround suppressed. Note that, in our model (as in (Rubin et al., 2015)), the
375 I cells have larger summation fields than the E cells (Fig. 3C,D). This means that there is
376 an intermediate range of stimulus sizes for which inhibitory firing rates continue on average
377 to increase with stimulus size, while excitatory cells are surround suppressed. With further
378 increase in stimulus size, both E and I cells are suppressed.

379 Result 2: Surround Tuning to the Center Orientation

380 Cells in V1 are found to be suppressed maximally when the surround stimulus orientation
381 matches the orientation of the center stimulus, regardless of whether that orientation matches
382 the cell's preferred orientation (Shushruth et al., 2012; Sillito et al., 1995; Trott and Born,
383 2015). This might enable the cell to detect orientation discontinuities or help in foreground-
384 background separation. A similar behavior has been observed for other stimulus features,
385 such as spatial frequency and velocity (Shen et al., 2007).

386 A previous model (Shushruth et al., 2012) showed that this behavior could arise if cells
387 received strong, weakly tuned excitatory and inhibitory input from the local network, while
388 the surround drove more strongly tuned inhibition of the excitatory cells and excitation
389 of the inhibitory cells. Then, when the center stimulus differed from the recorded cell's
390 preferred orientation, the cell would receive a great deal of local recurrent excitation and
391 inhibition from cells preferring the stimulus orientation, which would be the most strongly
392 activated cells. A surround stimulus matched to the center stimulus would most strongly
393 target these most activated cells. Withdrawal of input from those cells would then cause
394 greater suppression of the firing of the recorded cell than would direct suppression from
395 a surround stimulus at the cell's preferred orientation. Therefore, suppression would be
396 greatest when the surround stimulus orientation matched the center stimulus orientation.

397 We use similar reasoning here, but now in the context of the SSN model with power-law
398 rather than linear-rectified input/output functions. Our long-range projections are excitatory
399 onto both E and I cells, whereas in (Shushruth et al., 2012) they were inhibitory onto E
400 cells and excitatory onto I cells. In addition, the model of (Shushruth et al., 2012) was
401 not recurrent, because the input from one cell to another was simply determined by the
402 difference in their preferred orientations, regardless of the firing rate of the presynaptic cell
403 (and thus was a constant, independent of the stimulus); and the surround input to a cell was
404 determined only by the difference between the cell's preferred orientation and the surround
405 stimulus orientation, and not by the firing rates of lateral cells responding to the surround

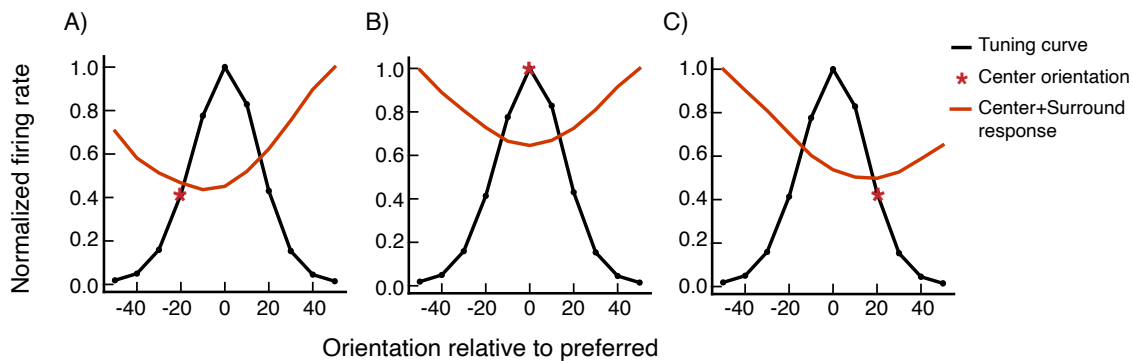


Figure 6: Surround tuning to the center orientation in an excitatory (E) cell The orientations are relative to the cell's preferred orientation. The black curves show the cell's orientation tuning curve for a center-only stimulus (*i.e.*, firing rate vs. center orientation), normalized so the maximum response is 1.0. The red curves show the similarly normalized tuning to surround orientation for a fixed center stimulus. In each panel, the red asterisk marks the fixed center orientation: (A) center at preferred minus 20°, (B) center at preferred and (C) center at preferred plus 20°.

406 stimulus. We use a recurrent model.

407 We record the firing rate of cells in the network for different center orientations. For each
408 center orientation, we then present a stimulus in the surround, rotate its orientation, and
409 record the cell's firing rate for each center-surround orientation configuration. In an exci-
410 tatory cell (Fig. 6), we study tuning to center orientation absent a surround (black curves)
411 and then tuning to surround orientation for a fixed center stimulus (red curves). The most
412 suppressive surround orientation (minimum of red curve) is pulled strongly toward the center
413 orientation (red asterisk) as the center orientation is varied from -20° relative to preferred
414 orientation (Fig. 6A), to preferred (Fig. 6B), to +20° relative to preferred (Fig. 6C). Similar
415 results are seen more generally in 67 excitatory cells at randomly selected grid locations
416 (Fig. 7). The surround orientation producing maximum suppression is pulled strongly to-
417 wards the center orientation (Fig. 7A,C-D) and in most cases is within 10° of the center
418 orientation (Fig. 7B).

419 As described above, surround tuning to the center orientation arises due to the strong,
420 broadly tuned local connectivity profile in orientation space, along with the more sharply
421 tuned surround input, which causes maximal input to the cell to come from cells preferring
422 the center stimulus rather than from cells with the same preferred orientation as the recorded

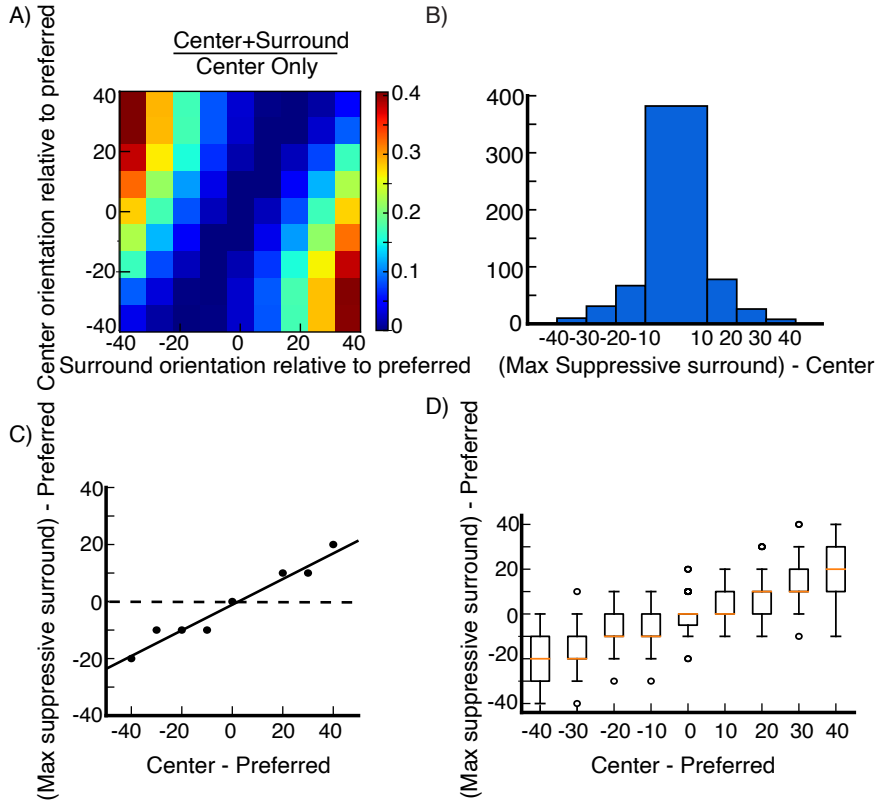


Figure 7: Surround tuning to the center orientation Surround tuning in 67 excitatory (E) cells at randomly selected grid locations (see section Model Details). Both center and surround orientations are varied from preferred minus 40° to preferred plus 40° in increments of 10° . (A) Average surround modulation map. For each cell, the map is obtained by dividing center-surround responses by the corresponding center-only responses, each row has its minimum value subtracted. (B) Histogram of the difference between the orientation of the surround that maximally suppresses the cell's firing rate, and the center stimulus orientation. The data is pooled over all cells and center orientations. (C) Orientation of the surround that maximally suppresses the cell's firing rate plotted against the center stimulus orientation, averaged over all cells. (D) Whisker plot of orientation of the surround that maximally suppresses the cell's firing rate against the center stimulus orientation, the box extends from quantile Q1 to Q3, the orange line is the median. The upper whisker extends to last datum less than $Q3 + k \cdot IQR$, similarly, the lower whisker extends to the first datum greater than $Q1 - k \cdot IQR$, where IQR is the interquartile range ($Q3 - Q1$) and $k = 1.5$, the circles represent the outlier data. In (A), (C), (D), orientations are shown relative to preferred.

423 cell. This makes suppression targeted to cells preferring the center stimulus more potent than
 424 suppression targeted to cells preferring the recorded cell's own preferred orientation.

425 Result 3: Feature-Specific Surround Suppression

426 Surround suppression in V1 is not blind to the center stimulus, as we have just seen. This also
427 manifests in the *feature-specificity* of surround suppression (Trott and Born, 2015): if multiple
428 stimuli are present in the cell's center, the surround more strongly suppresses the response
429 component driven by the center stimulus whose orientation matches the surround's. We test
430 whether V1 lateral connections can mediate such computation. We follow the procedure
431 described in Trott and Born (2015).

432 We record the firing rate of a small population of neurons to each of two oriented gratings.
433 For each stimulus, we fit the average response vs. preferred orientation across the population
434 with a Von Mises function, call these functions P_1 and P_2 (Fig. 8A). We then record the
435 population's firing rates to a center plaid stimulus, the superposition of the two individual
436 gratings. If the two gratings differ by, *e.g.*, 60° , we will call this a 60° plaid or a plaid angle
437 of 60° . We fit the population's response to the plaid stimulus as a linear combination of the
438 two components, $R_{\text{plaid}} = w_1 P_1 + w_2 P_2$.

439 We then introduce a surround stimulus whose orientation matches the second component
440 of the plaid center stimulus, and measure the new values of w_1 and w_2 . We repeat the same
441 procedure as we rotate the plaid, each time matching the surround stimulus to the orientation
442 of the 2nd plaid component. For responses to a 60° plaid alone, w_1 and w_2 on average have
443 about equal strength, but the addition of a surround stimulus matched to the second plaid
444 component suppresses w_2 much more than w_1 (Fig. 8B,C).

445 We carry out this experiment for different plaids, with plaid angles $[-60^\circ, -30^\circ, 0^\circ, 30^\circ,$
446 $60^\circ, 90^\circ]$. The mean values of w_1 and w_2 across all of these plaids cluster around $w_1=w_2$
447 for the plaid stimulus alone (Fig. 9A), but are heavily shifted towards w_1 when the surround
448 stimulus matched to the second plaid component is added (Fig. 9B). In Fig. 9C we show
449 the mean values of data points in Fig. 9A,B for each plaid angle. In the absence of a sur-
450 round stimulus there is no difference between w_1 and w_2 . When a surround stimulus with
451 orientation matching the plaid's second component is introduced, both components of the

452 plaid are suppressed, however, we clearly see that the second component is suppressed more.
 453 Hence, the surround stimulus suppress mostly the center stimulus component that has sim-
 454 ilar feature. In our model, this phenomena emerges because long range lateral connections
 455 connect cells with similar preferred orientations. The surround stimulus mostly excite cells
 456 with preferred orientation close to its orientation. These cells in turn will mostly suppress
 457 the cells at the center which have similar preferred orientation. Finally, we point out that
 458 the results remain the same if we repeat the same experiment and record from a single cell
 459 rather than from a small local population.

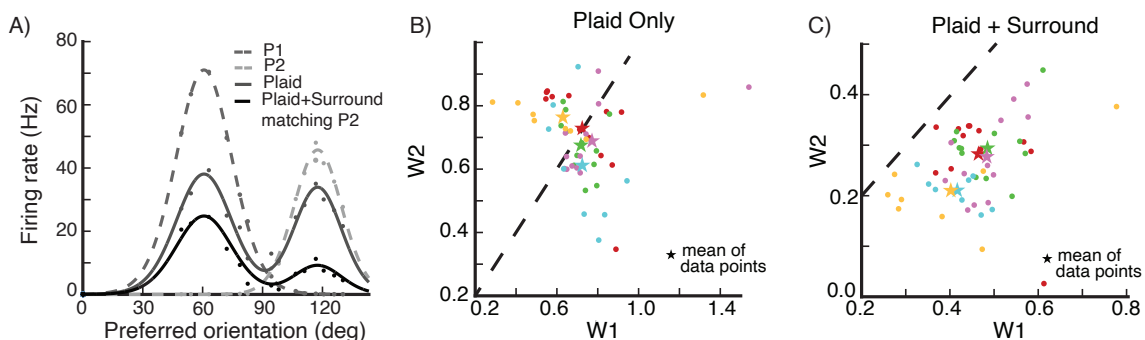


Figure 8: Feature-specific surround suppression (A) The firing rate of a small population of neurons in response to a center stimulus. The neurons are binned in 5° bins according to their preferred orientation. The dots are the data points, and the lines are the Von-Mises-function fits to the data. The medium gray points and dashed line are the population response to the first component of the plaid (P₁). The light gray points and dashed line are the population response to the second component of the plaid (P₂). The dark gray points and solid line are the population response to the plaid. The black points and solid line are the population response to the plaid in the presence of a surround stimulus whose orientation matches the plaid's second component. (B,C) values of w₁ and w₂ (the weightings in fitting the plaid population response to a weighted sum of the two component responses), for a 60° center plaid stimulus, shown for 12 different plaid rotations (every 10°), recorded from five different populations (indicated by colors). The populations are centered around randomly selected grid locations (see section Model Details). Missing data points imply that we can not find a good fit of the data for certain stimulus configurations. The star symbols are the mean values of w₁ and w₂ for each location. (B) Responses to plaid center stimulus only. (C) Responses to plaid center stimulus in the presence of a surround stimulus with orientation equal to the plaid's second component. Dashed lines are unit diagonals, along which w₁=w₂

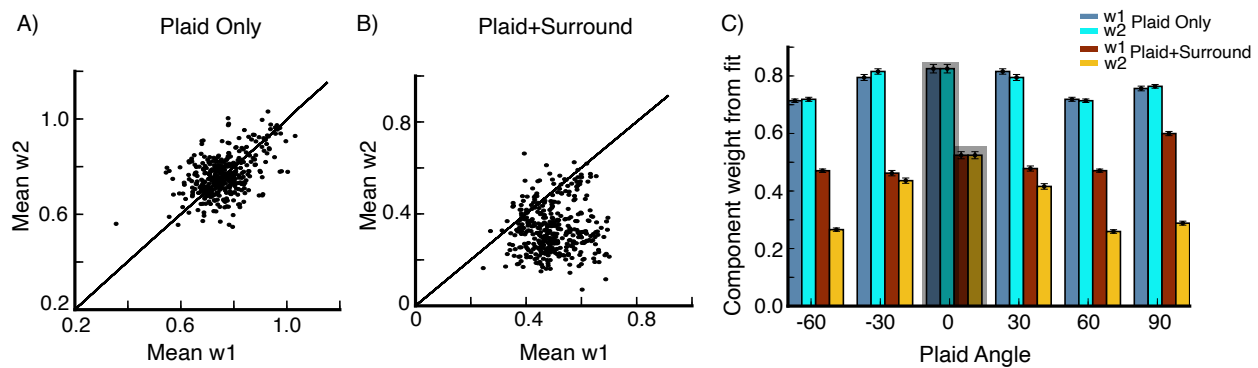


Figure 9: Feature-specific surround suppression (A,B) Mean w_1 is plotted against mean w_2 for plaid angles $[-60^\circ, -30^\circ, 30^\circ, 60^\circ, 90^\circ]$ from 80 populations, centered around 80 randomly selected grid locations (see section Model Details). The mean values of w_1 and w_2 are obtained from averaging data for different rotations of the plaid (A) for plaid center stimulus only (B) for plaid center stimulus in the presence of surround stimulus with orientation equal the plaid's second component. (C) Mean values of the data points in (A) and (B) for different plaid angles, we also include the data for plaid angle 0° , error bars are the s.e.m.

460 Result 4: Activity Decay Time

461 While exciting V1 with a visual stimulus, Reinhold et al. (2015) abruptly silenced the tha-
 462 lamic input to V1, by silencing the lateral geniculate nucleus (LGN) through optogenetic
 463 stimulation of the thalamic reticular nucleus (TRN). They showed that, after thalamic si-
 464 lencing, the cortical activity in V1 exhibited a fast decay, two orders of magnitude faster
 465 than the decay after visual stimulus offset. The authors called this decay time after thalamic
 466 silencing the cortical decay function (CDF). The CDF across all V1 layers was of the order
 467 of 10 ms, in particular for multiunits the CDF + s.e.m. was L2/3: 9.8 ± 1.7 ms, L4: 9.0 ± 2.2
 468 ms, L5a: 8.9 ± 1.3 ms, L5b: 15.7 ± 2.5 ms and L6: 7.6 ± 1.5 ms. The CDF was almost the
 469 same in awake and anesthetized mice. Furthermore, the authors found that the CDF was
 470 independent of the stimulus contrast.

471 We test if the dynamics in our network are in agreement with what has been reported.
 472 Since we only model layer 2/3 in V1, silencing LGN is equivalent to the removal of the
 473 feedforward input in our model. We record the activity of a cell for two stimulus sizes 2° and
 474 10° , each at two contrast levels, high contrast (C=17) and low contrast (C=9). In all cases,

475 the feedforward input is removed at 200 ms. To obtain the activity decay time constant, we
476 fit the decaying activity with an exponential function. We find the decay time constant for
477 the excitatory cells to be roughly 10 ms, which is in agreement to what has been reported
478 in Reinhold et al. (2015) as we show in Fig. 10. For 50 excitatory cells at randomly selected
479 grid locations, the activity decay time constant (mean \pm s.e.m.) for a 2° stimulus at high
480 contrast is 10.04 ± 0.01 ms and at low contrast is 9.99 ± 0.02 ms, and for a 10° stimulus at
481 high contrast 9.75 ms and at low contrast 9.76 ms (when we do not report it, the s.e.m. is too
482 small). The activity decay time constant is almost independent of the stimulus contrast level
483 and size. It is roughly given by the excitatory cells' time constant in the model. Similarly, the
484 activity decay time scale for the inhibitory cells is roughly given by the inhibitory cells' time
485 constant. For 2° stimulus at high contrast the inhibitory cells activity decay time constant
486 is 6.93 ± 0.01 ms and at low contrast 6.73 ± 0.04 ms, and for the 10° stimulus at high contrast
487 it is 6.69 ± 0.03 ms and at low contrast 6.98 ± 0.05 ms.

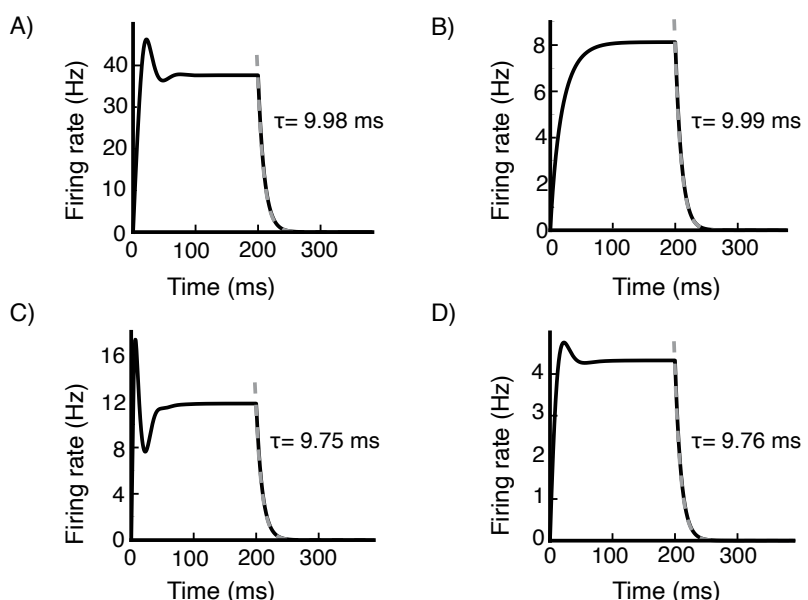


Figure 10: Activity decay time The time response of an excitatory (E) cell at a randomly selected grid location (see section Mode Details) for various stimulus conditions. (A) and (B) 2° size stimulus at high contrast (C=17) and low contrast (C=9) respectively. (C) and (D) 10° size stimulus at high contrast (C=17) and low contrast (C=9) respectively. The feedforward input is removed at 200 ms. The activity decay time constant is obtained by fitting an exponential function to the decaying activity. The activity decay time constant is roughly independent of the stimulus contrast level and size.

488 Result 5: Conductance-based Spiking Model

489 To test whether our results depend on the neuron model, we replace the rate units in the
490 network with conductance based spiking units (Eq. 7 in section Model Details). To make
491 the model more biologically realistic, we assume the excitatory and the inhibitory cells have
492 spontaneous activity levels of 1.5 Hz and 3 Hz respectively. We first show how the input
493 currents to a cell and its firing rate change with external drive (Fig. 11A,B). The net input
494 current a neuron receives increases rapidly as a function of external current for weak external
495 input, but sublinearly for stronger external input (Fig. 11A). The network input becomes
496 increasingly inhibitory with increasing external drive (Fig. 11C).

497 Most of our key findings in the rate model also hold in the spiking model. Both excitatory
498 cells and inhibitory cells are surround suppressed, the excitatory cells are more strongly
499 surround suppressed than the inhibitory cells as we see from the length tuning curves for
500 6 E cells (Fig. 12 top panel) and 6 I cells (Fig. 12 lower panel), and the average size tuning
501 across 30 E cells and 30 I cells at the same grid locations (Fig. 13 A,B). The strength of
502 surround suppression increases with increasing stimulus contrast (Fig. 12 and Fig. 13 A,B).
503 To compute the suppressive index (SI), we fit the cells responses with a double Gaussian
504 function. The mean SI is 0.45 ± 0.07 for the excitatory cells and 0.098 ± 0.054 for the
505 inhibitory cells at $C=10$, and increases to 0.65 ± 0.09 and 0.14 ± 0.06 at $C=100$.

506 We also show the distribution of the summation field sizes of the 30 E cells selected above
507 for two contrast levels $C=100$ and $C=10$ in Fig. 13C. The summation field size decreases with
508 increasing contrast (Fig. 13D).

509 To test whether surround suppression in the spiking network is also accompanied by a
510 decrease in excitation and inhibition, as reported by Ozeki et al. (2009), we plot the excitatory
511 conductance values (Fig. 14A) and the inhibitory conductance values (Fig. 14B) for the same
512 30 E cells for a large stimulus for which all the cells are suppressed against their values for
513 a small stimulus around which the cells respond maximally (we pick the size of the small
514 stimulus using the same method described in Result 1). Both excitatory and inhibitory

515 conductances are smaller for the large suppressive stimulus.

516 The results for feature-specific surround suppression are qualitatively similar to what we
 517 observe in the rate model, Fig. 15B is the same as Fig. 9A,B. For surround tuning to the
 518 center orientation, even though we can see a trend in some cells similar to that we observe in
 519 the rate model, overall the phenomenon is weak for the center stimulus orientations that give
 520 a response above the spontaneous activity level, Fig. 15A shows the surround modulation
 521 map in the spiking model. We point out that we do not optimize the model parameters, so a
 522 different set of values of the connectivity profile parameters, such as the width of connectivity
 523 in orientation space and the length of connections, may lead to better results as we have
 524 observed in a few simulations. Also, the conductances values are not fine tuned, so a different
 525 set of values can for example give larger SI indexes while still producing result 3.

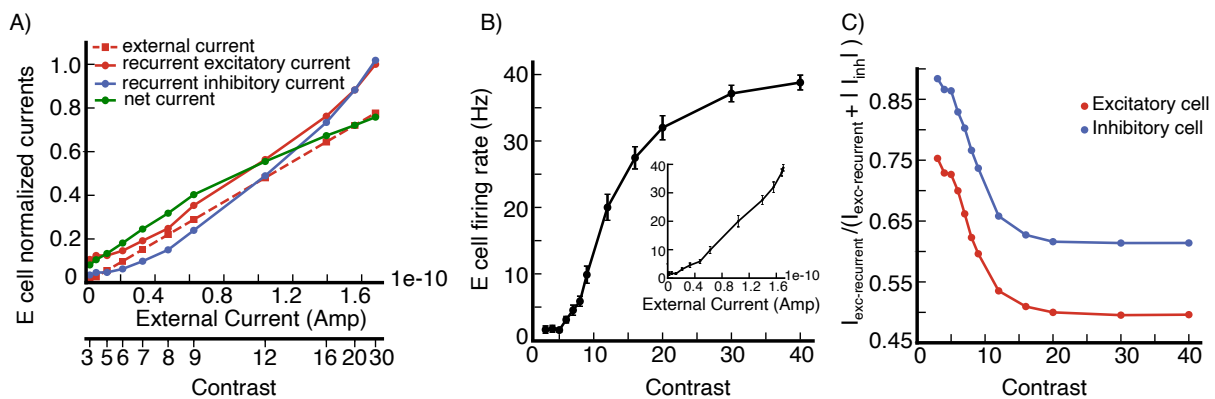


Figure 11: Conductance-based spiking model (A) Input currents to an excitatory (E) cell at a randomly selected grid location (see section Model Details) vs external input current. The recurrent excitatory current $I_{exc\text{-}recurrent} = \langle g_E(R_E - V) \rangle_t$, the recurrent inhibitory current is the absolute value of $I_{inh} = \langle g_I(R_I - V) \rangle_t$ and the external current $I_{ext} = \langle g_{in}(R_E - V) \rangle_t$ where $\langle \rangle_t$ denotes time average. The net current is $(I_{ext} + I_{exc\text{-}recurrent} + I_{inh})$, note that I_{inh} is negative in the spiking model. All currents are normalized to the peak value of the recurrent excitatory current. Stimulus contrast level corresponding to the external current is shown on the bottom axis. (B) Firing rate of the cell in (A) vs contrast. (C) $I_{exc\text{-}recurrent} / (I_{exc\text{-}recurrent} + |I_{inh}|)$ vs contrast for the cell in (A) and an inhibitory cell at the same grid location. In these experiments we use a stimulus with diameter 2.16° and orientation equal to the cell's preferred orientation.

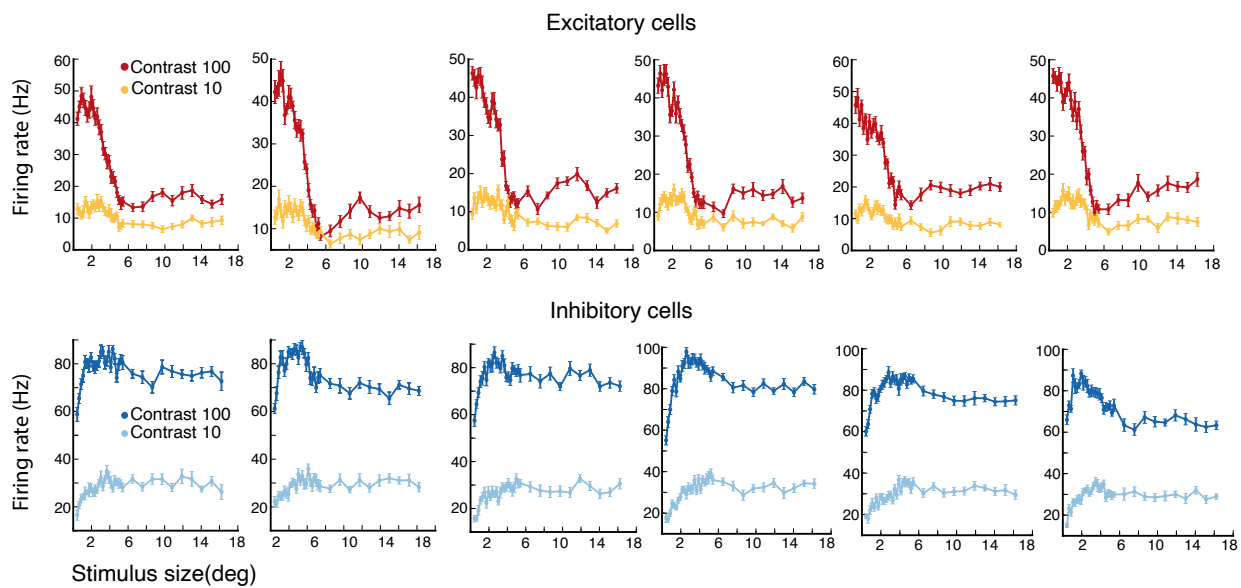


Figure 12: Conductance-based spiking model, surround suppression Length tuning curves of 6 excitatory (E) cells (top panel) and 6 inhibitory (I) cells (lower panel) for two different stimulus contrast levels $C=100$ and $C=10$. The error bars are the s.e.m.

526 Discussion

527 In previous work (Ahmadian et al., 2013; Rubin et al., 2015) we showed that the stabilized
528 supralinear network motif (SSN) can explain normalization and surround suppression if
529 combined with simple connectivity profiles, in which connection strength decreases with
530 increasing distance across cortex or between preferred features. In Rubin et al. (2015) we
531 presented a 2-d SSN model of V1 as a proof of principle and showed that the model can
532 generate surround suppression. Ozeki et al. (2009) found that an iso-oriented surround
533 stimulus reduces the values of both excitatory and inhibitory conductances of surround
534 suppressed cells in cat V1. We have found that, unlike in the simpler models studied in
535 Rubin et al. (2015), the 2-d model did not show this phenomena.

536 In this paper we built a rate-based model of layer 2/3 of V1 of animals with orientation
537 maps and showed that lateral connections are capable of generating consistently a set of
538 phenomena that have been observed in V1, including surround suppression, surround tuning
539 to the center orientation and feature-specific suppression. We also showed that surround

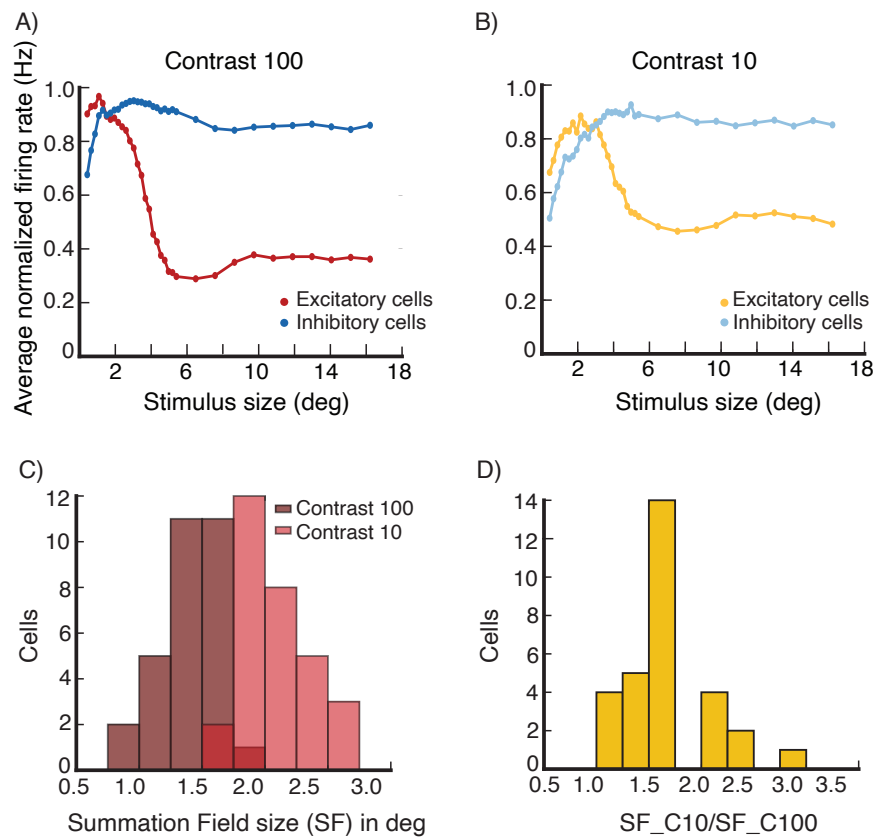


Figure 13: Conductance-based spiking model, surround suppression The average firing rate of 30 excitatory (E) cells at randomly selected grid locations (see section Model Details), and of 30 inhibitory (I) cells at the same grid locations, after normalizing each cell's rates so that its peak rate is 1.0, vs. stimulus size at contrast C=100 (A) and contrast C=10 (B). (C,D) Summation Field Sizes. (C) The distribution of summation field size of the 30 E cells used to produce panels (A) and (B) at contrasts C=100 (dark red color) and C=10 (light red color). (D) The distribution of the ratio of the summation field sizes in (C). The summation field size of all cells, is smaller at the higher contrast stimulus.

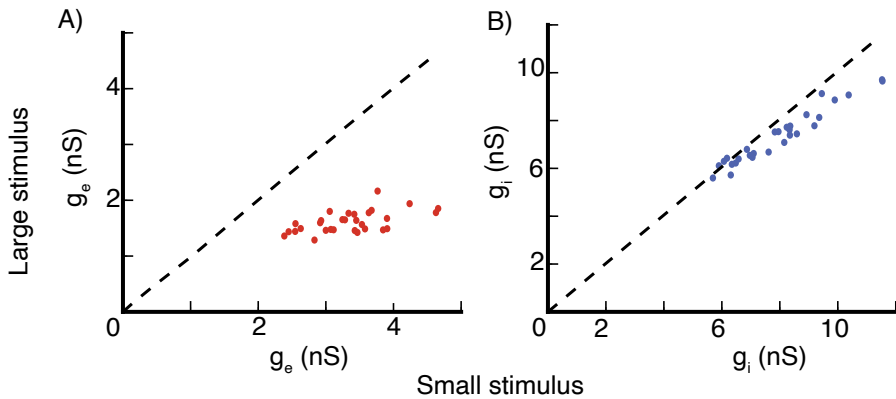


Figure 14: Conductance-based spiking model, surround suppression Excitatory and inhibitory conductances values of the 30 excitatory (E) cells used in Fig. 13. (A) Excitatory conductance values of the E cells for a large suppressive stimulus are plotted against their values for a small stimulus size around which the cells respond maximally. (B) same as (A) but for inhibitory conductances. Stimulus contrast $C=100$.

540 suppression is accompanied by a decrease in the excitatory and inhibitory inputs. As far as
541 we know, this is the only spatially extended model of V1 that has shown this phenomena.
542 The activity decay time constant for the excitatory cells in the model is fast, about the same
543 as the single-cell time constant, as in Reinhold et al. (2015). Finally, we showed that our
544 key results hold in a conductance-based spiking network.

545 The model gives insight into the circuit mechanisms that may underly the above observed
546 phenomena. The network is a stabilized supralinear network, it has specific connectivity high-
547 lighted by dense, strong local excitatory connections that are broadly tuned in orientation
548 space, and long range patchy excitatory connections that are biased toward inhibitory cells
549 at longer distances. The network is in a strongly nonlinear regime quantified by $\Omega_E < 0 < \Omega_I$
550 (Ahmadian et al., 2013). The requirement that the local connectivity be broadly tuned in
551 orientation space is essential to obtain surround tuning to the center orientation, but not to
552 obtain surround suppression and feature-specific suppression. We note that the parameters
553 we used, such as connectivity profile, input profile, and the underlying orientation map, were
554 chosen without tuning them to any of the phenomena we study.

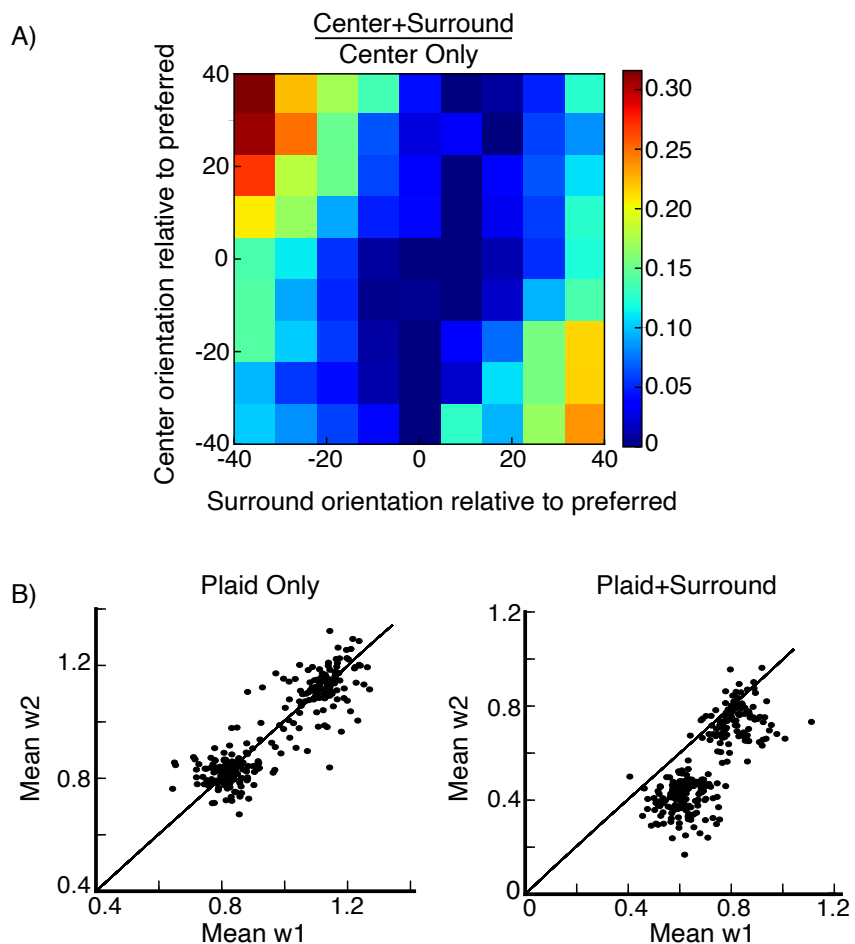


Figure 15: Conductance-based spiking model, surround tuning to the center orientation and feature-specific surround suppression (A) Surround tuning to the center orientation, average surround modulation map, the data is from 23 excitatory (E) cells at randomly selected grid locations (see section Model Details), same plot as Fig. 7A. (B) Feature-specific surround suppression, the data is from 56 populations centered around 56 randomly selected grid locations (see section Model Details), same plot as Fig. 9A,B.

555 Acknowledgments

556 We acknowledge computing resources from Columbia University's Shared Research Com-
557 puting Facility project, which is supported by NIH Research Facility Improvement Grant
558 1G20RR030893-01, and associated funds from the New York State Empire State Develop-
559 ment, Division of Science Technology and Innovation (NYSTAR) Contract C090171, both
560 awarded April 15, 2010. This project was supported by NIH grant R01-EY11001, grant
561 2016-4 from the Swartz Foundation, the Gatsby Charitable Foundation, and NSF NeuroNex

562 Award DBI-1707398. D. Obeid would like to thank Richard Born, Alexander Trott, S.
563 Shushruth and Cengiz Pehlevan for helpful discussions.

564 References

- 565 Adesnik, H. (2017). Synaptic mechanisms of feature coding in the visual cortex of awake
566 mice. *Neuron*, 95(5):1147–1159.
- 567 Ahmadian, Y., Rubin, D. B., and Miller, K. D. (2013). Analysis of the stabilized supralinear
568 network. *Neural computation*, 25(8):1994–2037.
- 569 Akasaki, T., Sato, H., Yoshimura, Y., Ozeki, H., and Shimegi, S. (2002). Suppressive effects of
570 receptive field surround on neuronal activity in the cat primary visual cortex. *Neuroscience
571 Research*, 43(3):207–220.
- 572 Albrecht, D. G. and Hamilton, D. B. (1982). Striate cortex of monkey and cat: contrast
573 response function. *Journal of neurophysiology*, 48(1):217–237.
- 574 Albrecht, G. (1991). Motion selectivity and the contrast-response function of simple cells in
575 the visual cortex. *Vis Neurosci*, pages 531–546.
- 576 Amir, Y., Harel, M., and Malach, R. (1993). Cortical hierarchy reflected in the organization
577 of intrinsic connections in macaque monkey visual cortex. *The Journal of Comparative
578 Neurology*, 334(1):19–46.
- 579 Angelucci, A., Bijanzadeh, M., Nurminen, L., Federer, F., Merlin, S., and Bressloff, P. C.
580 (2017). Circuits and mechanisms for surround modulation in visual cortex. *Annual review
581 of neuroscience*, 40:425–451.
- 582 Bair, W., Cavanaugh, J. R., and Movshon, J. A. (2003). Time course and time-distance
583 relationships for surround suppression in macaque v1 neurons. *Journal of Neuroscience*,
584 23(20):7690–7701.

- 585 Bosking, W. H., Zhang, Y., Schofield, B., and Fitzpatrick, D. (1997). Orientation selectivity
586 and the arrangement of horizontal connections in tree shrew striate cortex. *Journal of*
587 *neuroscience*, 17(6):2112–2127.
- 588 Carandini, M., Heeger, D., and Movshon, J. A. (1997). Linearity and normalization in simple
589 cells of the macaque primary visual cortex. *Journal of Neuroscience*, 17:8621–8644.
- 590 Carandini, M., Heeger, D. J., and Movshon, J. A. (1999). Linearity and gain control in v1
591 simple cells. In *Models of cortical circuits*, pages 401–443. Springer.
- 592 Cavanaugh, J. R., Bair, W., and Movshon, J. A. (2002). Nature and interaction of signals
593 from the receptive field center and surround in macaque v1 neurons. *Journal of neuro-*
594 *physiology*, 88(5):2530–2546.
- 595 Chen, Y., Anand, S., Martinez-Conde, S., Macknik, S. L., Bereshpolova, Y., Swadlow, H. A.,
596 and Alonso, J.-M. (2009). The linearity and selectivity of neuronal responses in awake
597 visual cortex. *Journal of vision*, 9(9):12–12.
- 598 Finn, I. M., Priebe, N. J., and Ferster, D. (2007). The emergence of contrast-invariant
599 orientation tuning in simple cells of cat visual cortex. *Neuron*, 54(1):137–152.
- 600 Gur, M. and Snodderly, D. M. (2008). Physiological differences between neurons in layer
601 2 and layer 3 of primary visual cortex (v1) of alert macaque monkeys. *The Journal of*
602 *physiology*, 586(9):2293–2306.
- 603 Hansel, D. and Van Vreeswijk, C. (2002). How noise contributes to contrast invariance of
604 orientation tuning in cat visual cortex. *Journal of Neuroscience*, 22(12):5118–5128.
- 605 Heeger, D. J. (1992). Half-squaring in responses of cat striate cells. *Visual neuroscience*,
606 9(5):427–443.
- 607 Kaschube, M., Schnabel, M., Löwel, S., Coppola, D. M., White, L. E., and Wolf, F.

- 608 (2010). Universality in the evolution of orientation columns in the visual cortex. *Science*, 330(6007):1113–1116.
- 610 Miller, K. D. and Troyer, T. W. (2002). Neural noise can explain expansive, power-law
611 nonlinearities in neural response functions. *Journal of neurophysiology*, 87(2):653–659.
- 612 Ozeki, H., Finn, I. M., Schaffer, E. S., Miller, K. D., and Ferster, D. (2009). Inhibitory stabi-
613 lization of the cortical network underlies visual surround suppression. *Neuron*, 62(4):578–
614 592.
- 615 Reinhold, K., Lien, A. D., and Scanziani, M. (2015). Distinct recurrent versus afferent
616 dynamics in cortical visual processing. *Nature neuroscience*.
- 617 Ringach, D. L., Shapley, R. M., and Hawken, M. J. (2002). Orientation selectivity in macaque
618 v1: diversity and laminar dependence. *Journal of Neuroscience*, 22(13):5639–5651.
- 619 Rubin, D. B., Van Hooser, S. D., and Miller, K. D. (2015). The stabilized supralinear
620 network: A unifying circuit motif underlying multi-input integration in sensory cortex.
621 *Neuron*, 85(2):402–417.
- 622 Sanzeni, A., Histed, M. H., and Brunel, N. (2020a). Emergence of irregular activity in net-
623 works of strongly coupled conductance-based neurons. *arXiv preprint arXiv:2009.12023*.
- 624 Sanzeni, A., Histed, M. H., and Brunel, N. (2020b). Response nonlinearities in networks of
625 spiking neurons. *PLoS computational biology*, 16(9):e1008165.
- 626 Sceniak, M. P., Ringach, D. L., Hawken, M. J., and Shapley, R. (1999). Contrast’s effect on
627 spatial summation by macaque v1 neurons. *Nature neuroscience*, 2(8):733.
- 628 Shen, Z.-M., Xu, W.-F., and Li, C.-Y. (2007). Cue-invariant detection of centre–surround
629 discontinuity by v1 neurons in awake macaque monkey. *The Journal of physiology*,
630 583(2):581–592.

- 631 Shushruth, S., Mangapathy, P., Ichida, J. M., Bressloff, P. C., Schwabe, L., and Angelucci, A.
632 (2012). Strong recurrent networks compute the orientation tuning of surround modulation
633 in the primate primary visual cortex. *The Journal of Neuroscience*, 32(1):308–321.
- 634 Sillito, A. M., Grieve, K. L., Jones, H. E., Cudeiro, J., and Davis, J. (1995). Visual cortical
635 mechanisms detecting focal orientation discontinuities. *Nature*, 378(6556):492–496.
- 636 Stettler, D. D., Das, A., Bennett, J., and Gilbert, C. D. (2002). Lateral connectivity and
637 contextual interactions in macaque primary visual cortex. *Neuron*, 36(4):739–750.
- 638 Trott, A. R. and Born, R. T. (2015). Input-gain control produces feature-specific surround
639 suppression. *The Journal of Neuroscience*, 35(12):4973–4982.
- 640 Troyer, T. W. and Miller, K. D. (1997). Physiological gain leads to high isi variability in a
641 simple model of a cortical regular spiking cell. *Neural Computation*, 9(5):971–983.
- 642 Tsodyks, M. V., Skaggs, W. E., and Sejnowski, T. J. and McNaughton, B. L. (1997). Paradox-
643 ical effects of external modulation of inhibitory interneurons. *J. Neurosci.*, 17:4382–4388.
- 644 Tuckwell, H. (1988). *Introduction to Theoretical Neurobiology: Volume 2, Nonlinear and*
645 *Stochastic theories*. Cambridge University Press.
- 646 Wang, C., Bardy, C., Huang, J. Y., FitzGibbon, T., and Dreher, B. (2009). Contrast
647 dependence of center and surround integration in primary visual cortex of the cat. *Journal*
648 *of vision*, 9(1):20–20.